ADVANCED FUNCTIONAL MATERIALS
www.afm-journal.de

Dispersion State and Fiber Toughness: Antibacterial Lysozyme-Single Walled Carbon Nanotubes

*Daniel W. Horn, Geyou Ao, Maryse Maugey, Cécile Zakri, Philippe Poulin, and Virginia A. Davis**

Novel multicomponent fibers that include single-walled carbon nanotubes (SWNT) and lysozyme (LSZ) are reported. These fibers exhibit antibacterial and mechanical properties suitable for fabrics, clothing and technical textiles in medical environments. The challenging combination of several components in a single fiber material is achieved via fundamental studies on the phase behavior of aqueous LSZ–SWNT dispersions. The addition of molecular cationic surfactants proved to be critical to achieving stable liquid mixtures that can be spun into fibers. In the absence of the cationic surfactant tetradecyl trimethylammonium bromide (TTAB), depletion effects result in large aggregates at relatively low SWNT concentration. However, the addition of TTAB increases the concentration at which demixing occurrs by approximately one order of magnitude. Dry-spun fibers with significant antibacterial activity and toughness are obtained from LSZ–TTAB–SWNT dispersions combined with a polyvinyl alcohol (PVA) solution. Toughness is strongly affected by the initial dispersion state. The most remarkable fibers are produced from concentrated LSZ–TTAB–SWNT supernatants; they both have four times the toughness of spider silk and 70% of the native LSZ activity.

1. Introduction

It is well established that dispersion and load transfer are the key impediments to porting the remarkable properties of single-walled carbon nanotubes (SWNT) to macroscopic structures. Due to their smooth and highly polarizable side-walls, SWNT exist as crystalline ropes or bundles with a characteristic van der Waals interaction energy of approximately 0.5 eV nm^{-1} of parallel contact.[1] Since the length of SWNT is on the order of hundreds to thousands of nanometers, exfoliation of SWNT requires significant energy. Due to their amphiphilic nature and the potential for π–π interactions, enzymes can be effective carbon nanotube dispersants. The inclusion of enzymes in carbon nanotube dispersions also enables the production of materials with synergistic properties.

Since 2000, communicable illnesses have cost the United States approximately $304 billion and 111 million lost work days annually.[2] There is growing concern about the spread of disease through contact with contaminated surfaces. Lysozyme (LSZ), a naturally abundant enzyme, catalyzes the hydrolysis of the 1,4-β-glycosidic linkage between N-acetyl glucosamine and N-acetyl muramic acid found in the peptidoglycan layer of Gram-positive bacteria.[3] Research on the combination of LSZ with SWNT has shown that LSZ's tryptophan residue[4] has sufficiently favorable interactions with SWNT to enable dispersion of individuals at low concentration.[5,6] The retention of LSZ's natural antibacterial activity during dispersion with SWNT, has enabled the manufacture of coatings[6] and fibers[7] that combine the properties of SWNT with the antibacterial properties of LSZ.[7] Fibers are of great interest for applications in medical environments. They can be used for fabrics, clothing, medical devices and technical textiles in a variety of situations. In addition to their practical and widespread uses, fibers often exhibit better properties than other bulk materials because of the controlled orientation and structure within the fibers. However, spinning multicomponent fibers is particularly challenging. The relatively low SWNT concentrations achieved in aqueous LSZ dispersions to date has limited the range of processing conditions and material applications that could be achieved. Ideally, it would be possible to achieve spinning dispersions comprised of active enzymes and concentrated SWNT. However, the stabilization of such dispersions is difficult because depletion effects can induce aggregation phenomena. In addition, the dispersion has to remain stabilized in order to form a solid fiber material. Finally, the fiber should include, in addition to active components, a binder that provides mechanical strength. To date the only fibers including LSZ and SWNT were spun with DNA, which is not particularly mechanically strong as a fiber matrix material.

In this work, we develop the understanding of LSZ–SWNT dispersions to achieve systems at concentrations substantially higher than previously reported. Concentrating aqueous LSZ–SWNT dispersions by evaporation resulted in depletion effects which caused a well-defined phase transition characterized by a

Dr. D. W. Horn, Dr. G. Ao, Prof. V. A. Davis
Department of Chemical Engineering
Auburn University
212 Ross Hall, Auburn, AL 36849, USA
E-mail: davisva@auburn.edu
M. Maugey, Prof. C. Zakri, Dr. P. Poulin
Centre de Recherche Paul Pascal-CNRS
Université Bordeaux
115 Avenue Schweitzer, 33600 Pessac, France

DOI: 10.1002/adfm.201300221

dramatic increase in the number and size of SWNT aggregates as well as a change in viscoelasticity. Adjusting the LSZ:SWNT concentrations only modestly affected the concentration at which aggregation occurred. However, we found that the addition of the cationic surfactant tetradecyl trimethylammonium bromide (TTAB), dramatically increased dispersion stability. Wet solution spinning LSZ–TTAB–SWNT dispersions into an aqueous polyvinyl alcohol (PVA) bath resulted in overcoating of the LSZ which inhibited antibacterial activity. However, combining the dispersions with PVA solutions followed by dry spinning resulted in fibers with both exceptional toughness and antibacterial activity. A toughness of 660 J g^{-1}, four times that of spider silk, was achieved for fibers produced from dispersions prepared from concentrated LSZ–TTAB–SWNT supernatants. These results show that understanding colloidal interactions is key to designing macroscale materials from SWNT dispersions. This understanding allowed for engineering novel multicomponent fibers that combined toughness and antibacterial activity.

2. Results and Discussion

2.1. Phase Behavior

The ability of LSZ to disperse SWNT as individuals has been previously shown by Nepal et al. using a combination of UV-vis spectroscopy of the dispersion and both ellipsometry and atomic force microscopy (AFM) on dried coatings.[6] There is a minimum relative LSZ concentration needed to overcome the strong van der Waals forces of attraction between SWNT. Above that threshold, the direct, hydrophobic interaction between LSZ and SWNT allows for stability of low concentration LSZ–SWNT dispersions.[4]

Without centrifugation, LSZ–SWNT mixtures contain both bundles and individuals. The phase behavior of mixtures with several LSZ to SWNT ratios were evaluated by concentrating the initial dispersions. In each case, a marked phase transition, where the number and size of SWNT aggregates dramatically increased, was observed using optical microscopy. As shown in **Table 1**, this transition was also detected using the rheological parameter $tan(\delta)$ which is the ratio of the viscous modulus G'' to the elastic modulus G'. The sudden increase in aggregation was due to a depletion interaction between the roughly spherical LSZ and the cylindrical SWNT; the LSZ acts as a depletant and causes attractive interactions between the SWNT. This is similar to the depletion interactions of colloids and polymers. The decrease in $tan(\delta)$ across the transition at each volume ratio indicates an increase in the elasticity of the dispersion microstructure and reflects the presence of a chemical or physical LSZ network surrounding the depletion induced SWNT aggregates. The loss of SWNT mixing entropy resulting from phase separation into a SWNT rich phase and SWNT dilute phase was compensated by the reduction in LSZ excluded volume as the SWNT were packed together. This led to an increase in LSZ translational entropy. Due to the slow rearrangement of entangled SWNT, the system did not achieve true thermodynamic equilibrium. The amorphous aggregates observed in the SWNT-rich phase are believed to be the result of a kinetically arrested phase separation. Depletion is effective at any concentration of SWNT, however this attractive interaction induces a phase separation of the SWNT only when the LSZ concentration is sufficiently large. Therefore, there exists an optimum relative LSZ concentration range to achieve homogenous dispersions of stabilized SWNT.

To increase the SWNT concentration that could be achieved by evaporating LSZ–SWNT mixtures, and to reduce the number and size of depletion induced aggregates, 0.34 vol% TTAB was added to the initial mixtures. TTAB is a cationic surfactant with a positively charged ammonium bromide head group and a 14-carbon tail; it was chosen because it was shown not to inhibit lytic activity when conjugated with LSZ. As shown by Dolle et al., longer chain surfactants should be more strongly adsorbed and have a higher Krafft temperature. Therefore, longer chain surfactants such as cetylammonium bromide (CTAB) may be useful for minimizing depletion interactions.[8] However, CTAB was not investigated because it was shown to inhibit lysozyme's antibacterial activity. Interestingly, the shorter analog, dodecyl trimethylammonium (DTAB), also inhibited lysozyme's activity. It is unclear why these two analogs inhibited antimicrobial activity while TTAB did not. The effect of surfactant chain length on both LSZ–SWNT dispersion stabilization and antibacterial activity is an intriguing area for future research.

The authors are not aware of any literature on the interactions of cationic surfactants with biomolecule-SWNT complexes. However, surfactants have played a major role in the study and assembly of SWNT ever since their discovery.[9–11] Zeta-potential studies of surfactant stabilized SWNT have given insight into the possible interactions.[12] The likely mechanism of SWNT dispersion in the TTAB system is based on the surface charging of SWNT.[13] The hydrophobic tails of surfactant adsorb on SWNT, and the hydrophilic heads create an effective charge on the SWNT surface. This surface charge then creates an electric double-layer which induces an electrostatic repulsion that stabilizes the SWNT against aggregation from van der Waals forces as predicted by Derjaguin–Landau–Verwey–Overbeek (DLVO) theory.[14] Initial thoughts on surfactant interactions with SWNT focused on the surfactant wrapping the SWNT and creating cylindrical micelles with the hydrocarbon chains arranged along the SWNT sidewall. However, more recent studies using small-angle neutron scattering and density functional theory calculations suggest that the interaction is a random and disordered adsorption of surfactant molecule tails onto the SWNT surface. Regardless of

Table 1. Phase behavior transitions showing the increase in elasticity by the change in tan(δ) in addition to the monophasic and demixed LSZ and SWNT concentrations.

Dispersion (Volumetric Ratio)	Monophasic			Demixed		
	tan(δ)	SWNT [vol%]	LSZ [vol%]	tan(δ)	SWNT [vol%]	LSZ [vol%]
8.5:1.0 LSZ:SWNT Mixture	0.464	0.079	0.673	0.193	0.092	0.782
6.4:1.0 LSZ:SWNT Mixture	0.424	0.098	0.627	0.226	0.114	0.730
4.3:1.0 LSZ:SWNT Mixture	0.659	0.073	0.312	0.298	0.080	0.342
2.1:1.0 LSZ:SWNT Mixture	0.650	0.152	0.326	0.184	0.166	0.355

Table 2. The phase transition concentrations for each volumetric ratio showing the demixed concentration of SWNT and LSZ for LSZ–SWNT and LSZ–TTAB–SWNT dispersions.

Dispersion (Volume Ratio)	Demixed SWNT [vol%]	Demixed LSZ [vol%]
2.1:1.0 LSZ:SWNT Mixture	0.166	0.355
2.1:1.0 LSZ:SWNT Supernatant	0.075	1.057
0.9:1.2:1.0 LSZ:TTAB:SWNT Mixture	1.877	1.596
0.9:1.2:1.0 LSZ:TTAB:SWNT Supernatant	0.687	1.151

the exact morphology of SWNT interaction, the stabilization mechanism remains that of electrostatic repulsion between surfactant molecules leading to colloidal stability as described by DLVO theory. The interaction of cationic surfactants with LSZ has also been well studied.[15–17] It is generally accepted that the binding of TTAB to LSZ occurs by a combination of electrostatic and hydrophobic interactions. More specifically, Hayashi et al.[16] and Subramanian et al.[17] have shown through optical spectroscopy that the saturated TTAB tail binds with surface bound indole moieties of tryptophan, the phenolic moieties of tyrosine amino acid residues, and exposed carboxyl groups which have been ionized by the aqueous environment.

While the total interactions in the LSZ–TTAB–SWNT system are inherently complex and difficult to deconvolute, **Table 2** clearly shows the significant effect TTAB has on the phase behavior transitions of LSZ–TTAB–SWNT dispersions. Two types of dispersions were investigated. The mixtures refer to samples that did not undergo any centrifugation to remove bundles prior to being concentrated by slow evaporation. The supernatants refer to dispersions that were produced by centrifuging these initial mixtures and concentrating only the supernatant. The phase transition of LSZ–TTAB–SWNT was defined by the SWNT concentration at which the number and size of SWNT aggregates dramatically increased. The reason for this aggregation is believed to be analogous to that of LSZ–SWNT dispersions. Even in the presence of TTAB, depletion interactions can take place.[10] Table 2 shows the post-transition concentration for LSZ and SWNT for lowest LSZ:SWNT mixture and supernatant dispersions (largest relative quantity of SWNT) and LSZ–TTAB–SWNT mixture and supernatant dispersions. It should be noted that the concentration ratios of LSZ:SWNT for TTAB dispersions were significantly lower than for LSZ–SWNT dispersions. The LSZ–SWNT phase behavior indicated that decreasing the LSZ:SWNT ratio only slightly increased the concentration at which aggregation occurred. However, the addition of TTAB resulted in an order of magnitude increase in the monophasic SWNT concentration. Moreover, the use of TTAB as a stabilizing agent allowed the LSZ–TTAB–SWNT supernatant to maintain enough SWNT after centrifugation to show the depletion phase transition. In the absence of TTAB, the concentration of SWNT in the supernatant was so low that depletion was not observed with increasing concentration. In fact, the initial concentration was too low for analytical

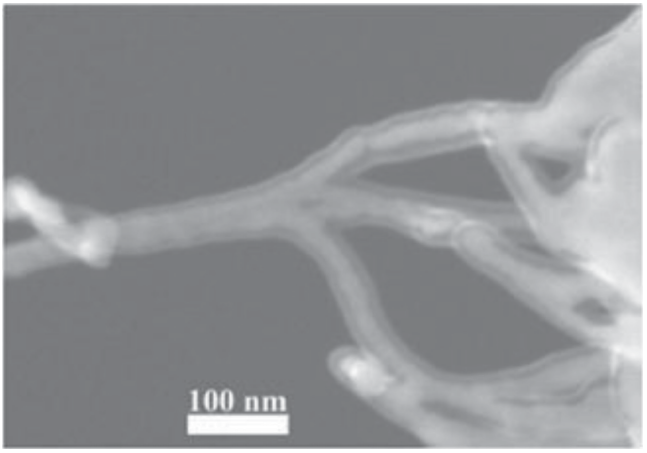

Figure 1. Scanning electron micrograph of a 0.24 vol% LSZ–0.34 vol% TTAB–0.28 vol% SWNT supernatant dispersion illustrating the interaction between SWNT (opaque) and LSZ-TTAB (translucent); magnification is 190 000×.

measurement; it was estimated from a dispersion mass balance. It is speculated that the increased size and total charge of the LSZ-TTAB complex compared with LSZ contributes to the stabilization. This hypothesis is supported by an increase in the zeta-potential from +24 mV for LSZ–SWNT to +31 mV for LSZ–TTAB–SWNT.

Scanning electron microscopy (SEM) of dried LSZ–TTAB–SWNT supernatant supported the interaction between LSZ, SWNT, and TTAB. **Figure 1** shows an opaque SWNT bundle surrounded by a semi-translucent layer of LSZ and TTAB. This layer appears similar to the LSZ layer previously reported in the absence of TTAB.[4] Energy dispersive x-ray spectroscopy (EDS) of six random locations of the translucent shell within Figure 1 showed an average elemental percentage of 11.8% bromine. This suggests that the presence of TTAB in the shell which would be consistent with studies on LSZ-TTAB interaction in the absence of SWNT.[16,17]

UV-vis spectroscopy of LSZ–TTAB–SWNT was performed to confirm the presence of SWNT individuals or small bundles within the dispersion and to reveal differences between the LSZ–SWNT and LSZ–TTAB–SWNT dispersions.

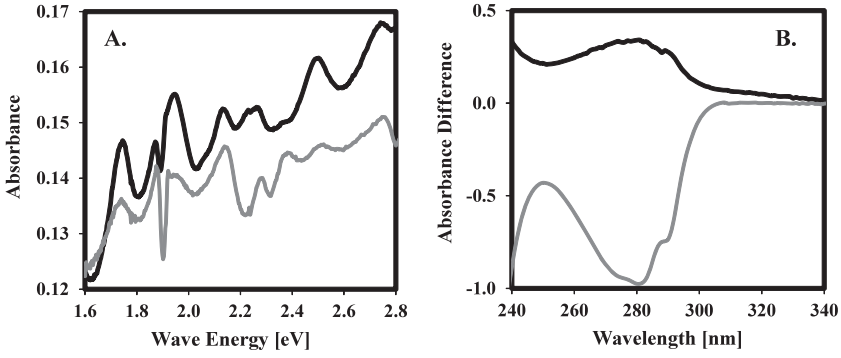

Figure 2. a) UV-vis spectroscopy of the supernatants of 0.24 vol% LSZ–0.28 vol% SWNT (gray) and 0.24 vol% LSZ–0.34 vol% TTAB–0.28 vol% SWNT (black) dispersions showing sharp van Hove singularity peaks between 1.6 and 2.4 eV, elucidating the ability of LSZ–TTAB solutions to disperse SWNT as individuals or small bundles; b) UV-vis difference spectra showing a change in the surroundings of the LSZ tryptophan chromophore.

Figure 2 shows UV-vis spectroscopy of the supernatants of 0.24 vol% LSZ–0.28 vol% SWNT and 0.24 vol% LSZ–0.34 vol% TTAB–0.28 vol% SWNT dispersions. Figure 2a shows sharp van Hove singularities between 1.6 and 2.4 eV for both dispersions, making clear the ability of LSZ-TTAB solutions to disperse SWNT as individuals or small bundles. The absorbance values of the LSZ–TTAB–SWNT dispersion at ≈1.6 eV have been shifted by 0.065 to coincide with the same wave energy absorbance values of the LSZ–SWNT dispersions. Shifting of the absorbance by an offset value was chosen over normalization, because normalization of the data would have led to smoothing and quenching of the peaks and prevented discerning the SWNT in LSZ–TTAB–SWNT dispersions. The offset was necessary due to the increased concentration of SWNT maintained in the LSZ–TTAB–SWNT supernatant. In addition to showing dispersibility, UV-vis also confirmed that the solvent environment surrounding the LSZ was different between the LSZ–SWNT and LSZ–TTAB–SWNT dispersions. Figure 2b shows the absorbance difference between the supernatants of 0.24 vol% LSZ–0.28 vol% SWNT and 0.24 vol% LSZ–0.34 vol% SWNT–0.28 vol% TTAB dispersions; absorbance values for a 0.24 vol% LSZ solution were subtracted to clarify the difference in the solvent environment of LSZ's tryptophan chromophore. Changes in the solvent surroundings are known to shift the absorbance intensity of a chromophore.[18] As previously reported, the hyperchromic shift for LSZ–SWNT is due to LSZ's tryptophan chromophore becoming more exposed to an aqueous environment as a result of opening to bind with the hydrophobic sidewall of SWNT in the aqueous dispersion.[4] The hypochromic shift seen for LSZ–TTAB–SWNT highlights the significant effect TTAB has on the tryptophan environment and suggests interaction between the hydrophobic tryptophan core and the hydrophobic TTAB tail.

2.2. Fiber Spinning

Attempts to solution spin LSZ–SWNT dispersions failed due to the presence of aggregates. Some small sections of fiber were obtained by wet spinning into a 1-butanol coagulation bath, but the mechanical properties were too poor to enable testing. Other dispersions and spinning methodologies resulted in fibers with more robust mechanical properties which are summarized in **Table 3**. The increased concentration at which aggregation occurred in LSZ–TTAB–SWNT mixtures enabled wet spinning into a PVA coagulation bath. This spinning method was chosen in an effort to capitalize on previous SWNT fiber spinning advances. PVA is believed to form an amorphous coating on SWNT and create an important interphase region which significantly improves mechanical properties.[10,19–21] Wet spinning of a dilute 0.24 vol% LSZ–0.28 vol% SWNT–0.34 vol% TTAB mixture into a rotating PVA coagulation bath resulted in fibers with smooth surfaces and cylindrical geometries that were mechanically robust enough for tensile testing. However, the 3.5 GPa Young's Modulus, 49.1 MPa tensile strength, and 3% strain to failure were unremarkable. In addition, coagulation had the unintended consequence of eliminating the fibers' antibacterial activity. Since PVA does not inhibit LSZ activity (see Section 2.3), it was hypothesized that the absence of antibacterial activity was the result of PVA physically overcoating LSZ on the fiber surface. To test this hypothesis, fibers were dry spun both in the absence of PVA and after mixing PVA directly into the spinning dope. Fibers dry spun from a 3.17 vol% LSZ–4.63 vol% TTAB–3.71 vol% SWNT mixture had antibacterial activity (see Section 2.3), but their Young's modulus and tensile strength were even an order of magnitude lower than the fibers coagulated in PVA. These poor mechanical properties were attributed to both a lack of elongational flow during spinning and the absence of PVA. In order to gain the elastic and elongational benefits of PVA without completely overcoating the LSZ, the dispersions were combined with a PVA solution prior to fiber spinning. However, exploration of numerous solvents failed to identify a potential coagulation bath for the resulting dispersions; salts were not tested since they could crystallize into the fiber matrix. Therefore, dry spinning was performed.

Dry spinning fibers from SWNT dispersions has typically failed due to either low solvent volatility or a lack of extensional viscosity. However, in this case, the presence of PVA in the spinning dopes enabled dry spinning onto Teflon surfaces. The PVA also had the added benefit of further improving dispersion stability. In fact, even LSZ–SWNT dispersions which did not contain TTAB could be spun after the addition of PVA; the resulting mechanical properties were even higher than for the LSZ–TTAB–SWNT fibers spun into a PVA coagulation bath. The inclusion of PVA is believed to have created a synergistic effect in increasing the mechanical properties of the fibers, as the contribution of pure PVA to the system is estimated at less than 1% of the mechanical strength.[22] In order to understand the influence of the dispersion state on fiber properties, LSZ–SWNT and LSZ–TTAB–SWNT mixtures and supernatants which were added to

Table 3. Mechanical properties of LSZ–SWNT and LSZ–TTAB–SWNT fibers from both wet and dry spun assembly methods illustrating the effect of dispersion state and processing method on the final mechanical properties.

Sample	Young's Modulus [GPa]	Tensile Strength [MPa]	Strain at Failure [%]	Toughness [J/g]
LSZ-TTAB-SWNT Mixture (0.24 vol.% – 0.34 vol.% – 0.28 vol.%) Wet Spun into 4.10 vol.% PVA	3.5 ± 0.5	49.1 ± 6.0	3.0 ± 0.7	–
LSZ-TTAB-SWNT Mixture (3.17 vol.% – 4.63 vol.% – 3.71 vol.%) Dry Spun	0.4 ± 0.0	4.5 ± 0.6	1.9 ± 0.3	–
LSZ-SWNT Mixture + PVA (0.71 vol.% – 0.16 vol.% + 10.21 vol.%) Dry Spun	22.3 ± 1.7	723.4 ± 47.5	3.7 ± 0.4	15.6
LSZ-SWNT Supernatant + PVA (0.36 vol.% – 0.03 vol.% in 9.99 vol.%) Dry Spun	26.3 ± 1.6	774.5 ± 53.0	37.6 ± 0.8	268.4
LSZ-SWNT-TTAB Mixture + PVA (1.00 vol.% – 1.44 vol.% – 1.17 vol.% + 9.68 vol.%) Dry Spun	32.0 ± 0.3	891.6 ± 30.5	61.2 ± 2.8	385.7
LSZ-SWNT-TTAB Supernatant + PVA (0.51 vol.% – 0.73 vol.% – 0.24 vol.% + 10.93 vol.%) Dry Spun	47.0 ± 1.4	1718.6 ± 93.7	86.9 ± 13.2	660.9

PVA were dry spun at the same conditions. For each composition, fibers from concentrated supernatants had higher mechanical properties than those produced from the concentrated mixtures even though the concentration of SWNT in the mixtures was higher. The poorer mechanical properties achieved when starting from a mixture are attributed to a larger number and size of aggregates in the dispersions creating inhomogeneities in the fibers.[23] In contrast, the more uniform microstructure of the concentrated supernatants enabled a more uniform fiber structure and better mechanical properties.

For fibers spun from dispersions that included PVA, the most notable differences were in the strain to failure and corresponding toughness. Fibers spun from concentrated LSZ–SWNT mixtures added to PVA had a low toughness of 15.6 J g^{-1}, but due to the better dispersion state, fibers from the corresponding supernatant had a toughness of 268.4 J g^{-1}. These values compare to 33 J g^{-1} for Kevlar and 165 J g^{-1} for spider silk.[19] The spinning dopes containing TTAB were remarkable because an even greater fiber toughness of 385.7 J g^{-1} was achieved even for the concentrated mixture which did not undergo any removal of bundles by centrifugation. Fibers spun from concentrated LSZ–TTAB–SWNT supernatant added to PVA solution had even better properties with a breaking strain of 86.9% and toughness of 660.9 J g^{-1}. This toughness is four times greater than that of spider silk and exceeds the record initially set by the Baughman group using gel spinning of surfactant stabilized SWNT into a PVA bath.[20] The Young's Modulus of 47 GPa and tensile strength of 1.7 GPa are also higher than that of spider silk, but lower than that of Kevlar and the strongest carbon nanotube fibers.[19] These results highlight the ongoing challenge of achieving high strength and toughness simultaneously. For example, the Windle group produced pure MWNT fibers by aerogel spinning that had a Young's Modulus of 3.6 GPa and tensile strength of 8.8 GPa, but for these fibers the toughness was only 121 J g^{-1}.[19]

The SEM images of fiber knots shown in **Figure 3** provide a qualitative indication of mechanical robustness.[19,11] All of the dry spun fibers appeared round initially, but flattened to a ribbon-like structure during to the drying process due to capillary forces. For LSZ–TTAB–SWNT mixed with PVA before dry spinning, the fiber surfaces ranged from that shown in Figure 3a to the very smooth surface in Figure 3b. Both dispersion state, and needle diameter appeared to affect the surface. Pottick showed with poly(p-phenylene benzobisthiazole) that increasing the pressure drop during extrusion modifies the surface morphology of fibers.[24] Based on preliminary investigations on the effect of needle diameter, it is believed that smaller diameters and increased pressure drop result in smoother LSZ–TTAB–SWNT-PVA fiber morphologies.

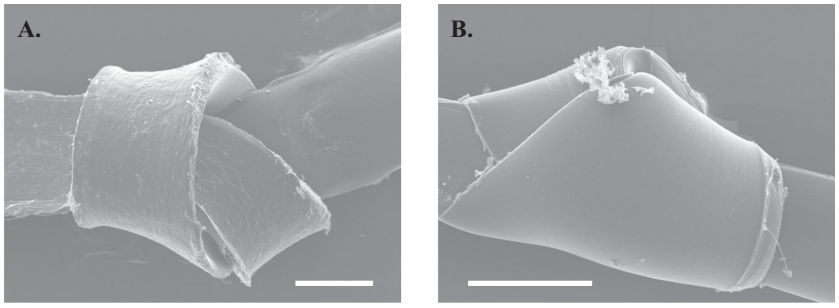

Figure 3. Scanning electron micrographs showing the mechanical robustness (knot) and smooth surface morphology of a) 1.00 vol% LSZ–1.44 vol% TTAB–1.17 vol% SWNT mixture in 9.68 vol% PVA fiber extruded from a 0.84 mm diameter needle and b) 0.51 vol% LSZ–0.73 vol% TTAB–0.24 vol% SWNT supernatant in 10.93 vol% PVA fiber extruded from a 0.26 mm diameter needle. The scale bar shown in each image is 500 nm.

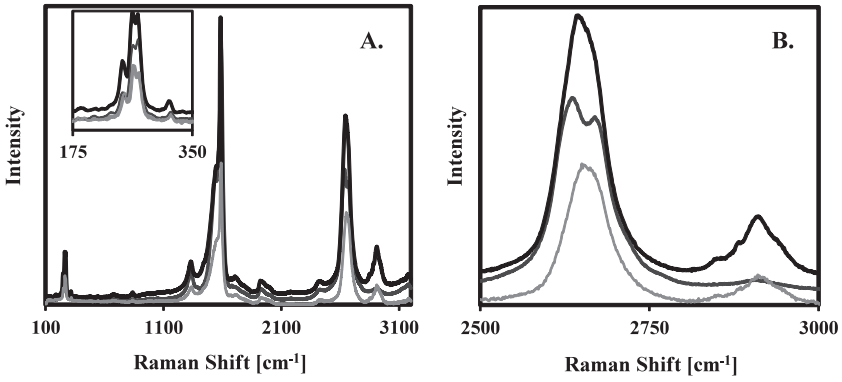

Figure 4. a) Raman spectra of SWNT film and LSZ–TTAB–SWNT-PVA mixture and supernatant fibers using a 514 nm excitation laser. Inset magnifies the RBM region. b) Magnified Raman spectra better showing the shifts in the G′-peak and characteristic CH_2 stretch associated with the polymer backbone stretching of PVA. Dark Gray (middle): SWNT. Black (top): Fiber from a LSZ–TTAB–SWNT mixture added to PVA solution. Light Gray (bottom): Fiber from a LSZ–TTAB–SWNT supernatant added to PVA solution.

Raman spectroscopy using both 514 nm and 785 nm lasers was performed on the SWNT and fibers produced from LSZ–TTAB–SWNT mixtures and supernatants mixed into PVA. The 514 nm laser data shown in **Figure 4** is of particular interest as it probes the LSZ–SWNT system as well as the PVA polymer backbone (data for the 785 nm laser may be found in the Supporting Information). Figure 4a shows characteristic radial breathing modes (RBM) from 100 cm^{-1} to 400 cm^{-1}, the D peak due to sp^3 hybridized carbons at ≈1335 cm^{-1}, the G peak due to tangential sp^2 hybridized carbons at ≈1589 cm^{-1}, and the G′ peak at ≈2645 cm^{-1} which is the second overtone of the D peak. The polymer backbone of the PVA present in each fiber resulted in the peaks at ≈2910 cm^{-1} (Figure 4b).[25] As summarized in **Table 4**, several facets of the Raman spectra support the existence of noncovalent functionalization of individual SWNT with LSZ-TTAB complexes. The D:G ratios varied only slightly between SWNT (0.126), LSZ–TTAB–SWNT supernatant (0.121), and LSZ–TTAB–SWNT mixture (0.147), indicating a noncovalent interaction. Charge transfer was evidenced by the G′-peak. Both the G[26] and G′[27,28] peaks have been used to indicate doping effects. For the data collected

Table 4. Raman spectroscopy data for 514 nm excitation laser. The changes in G′-peak position coupled with the decrease in G:G′ indicate charge transfer between SWNT and LSZ-TTAB complex present in each fiber.

	514 nm Laser							
Sample	D-Peak		G-Peak		G′ Peak		D/G	G/G′
	Shift [cm^{-1}]	Intensity	Shift [cm^{-1}]	Intensity	Shift [cm^{-1}]	Intensity		
SWNT	1338	4339	1589	34316	2636	18070	0.126	1.90
LSZ-TTAB-SWNT Supernatant + PVA	1338	2289	1589	18928	2650	12278	0.121	1.54
LSZ-TTAB-SWNT Mixture + PVA	1332	5668	1586	38497	2646	25287	0.147	1.52

here, charge transfer is best elucidated by the G′-peak shift as well as a decrease in G:G′ since the G′-peak position is independent of tensile load transfer.[28,29] Charge transfer for the present system was expected due to the presence of the quaternary ammonium ion. The lack of a shift in the G-peak could be explained by a combinatorial effect of charge transfer causing an upshift in frequency and tensile load transfer causing a downshift in frequency,[30] or the presence of the bromide counterion. The presence of tensile load transfer is supported by the increase in mechanical properties for LSZ–TTAB–SWNT in PVA. Another interesting aspect of the Raman spectra is the shifting of the RBM peak positions as shown in the inset of Figure 4a. There are several possible reasons for these shifts. The addition of TTAB to the LSZ–SWNT results in significant debundling of the SWNT as evidenced by the van Hove singularities shown in Figure 2a. This debundling of SWNT has been reported to result in shifting of RBM peaks.[31] In addition, it has been shown that changes in aggregation state result in different chirality SWNT being in resonance with a fixed-wavelength laser.[32] Finally, charge transfer has been linked to shifts in the RBM peaks.[33]

2.3. Antibacterial Activity

Turbidimetric analysis of antibacterial activity was performed on all LSZ–SWNT and LSZ–TTAB–SWNT dispersions and fibers by measuring the change in absorbance at 450 nm in an 0.015 wt% solution of *Micrococcus lysodeikticus* buffered with KOH. In order to determine the contribution of each constituent and the contribution of the interactions, all individual constituents were tested for activity. **Figure 5**a shows the activity analysis for water, LSZ, TTAB, PVA, LSZ-TTAB, and LSZ-PVA solutions. The decrease in absorbance for all solutions containing LSZ shows that they possessed lytic activity. The relatively constant absorbance for water, aqueous TTAB and aqueous PVA show these materials did not possess activity. The similar lysis rates for LSZ-TTAB and LSZ-PVA confirmed the non-inhibitory nature of TTAB and PVA toward the native activity of LSZ. After processing of LSZ–TTAB–SWNT dispersions and fibers, turbidimetric analysis was done to determine the effect of dispersion state and processing on the LSZ activity in each dispersion and fiber. Figure 5b shows the activity of each dispersion and fiber as a percentage of native LSZ activity maintained (each sample was normalized for the amount of LSZ present based on TGA measurements). The initial LSZ–SWNT dispersions had over 99% of the native LSZ activity. This is greater than that observed by Ding et al. who achieved a maximum of 90% of native LSZ activity in the presence of silica nanotubes.[34] Merli et al. found that covalently bonding LSZ to MWNT via EDC/NHS actually increased activity;[35] however, covalent functionalization has the disadvantages of reducing SWNT mechanical and electrical properties.[36] The activity of the supernatants being lower than those of the mixtures was most likely due to the removal of excess LSZ during centrifugation. Some studies have shown SWNT may have inherent antimicrobial activity; therefore, the reduced SWNT concentration may also have contributed to the reduced activity in the supernatant. The LSZ–TTAB–SWNT dispersions show a similar trend as the LSZ–SWNT dispersions, however, the supernatant loses less activity. At this time, the reason for this decreased loss in activity is unknown. It may due to a synergistic interaction between LSZ, SWNT, and TTAB, since there was no indication of any such relationship between the LSZ and TTAB as seen in Figure 5a. The concentrated mixture LSZ–TTAB–SWNT fiber maintains the highest degree of activity when compared with the LSZ–TTAB–SWNT fibers in PVA. This is likely due to the increased steric hindrance caused by incorporation of PVA inhibiting the interaction of the LSZ active site with the bacterial cell wall. It should be noted that

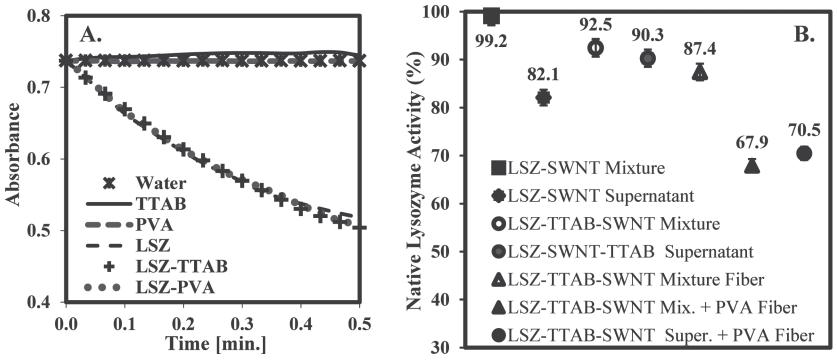

Figure 5. a) Turbidimetric analysis of all individual constituents present within LSZ–TTAB–SWNT macroscopic assemblies showing non-inhibitory effect of TTAB and PVA on native LSZ activity. b) Lytic activity analysis of LSZ–SWNT dispersions and LSZ–TTAB–SWNT dry spun fibers. Activity was tested against *M. lysodeikticus*. It should be noted that the calculated error for each sample was less than that of the UV-vis, therefore, the error shown is that inherent of the UV-vis used in characterization.

the loss in activity from LSZ–SWNT mixture dispersion to the resultant fiber (not shown) is approximately 60%, whereas the loss in activity from LSZ–TTAB–SWNT mixture to the least active resultant fiber is approximately 32%. The reason for this is unclear, however, likely involves the increased stability of the LSZ–TTAB–SWNT dispersions over the LSZ–SWNT dispersions. Overall, although there is a loss in activity, this data confirms the ability to process LSZ–SWNT dispersions into fibers which maintain antibacterial activity. Furthermore, it should be noted that a commercially available mouthwash containing LSZ maintains only 28.5% of native LSZ activity.[37] Therefore, although the loss of activity in LSZ–SWNT fibers seems significant, it is less than that of currently available commercial products.

3. Conclusions

This work highlights the importance of colloidal interactions and dispersion state for spinning fibers from SWNT dispersions. Initial efforts to produce LSZ–SWNT fibers were frustrated by depletion attraction resulting in demixing into a SWNT rich aggregate phase and a SWNT poor aqueous LSZ phase. The incorporation of TTAB greatly improved dispersion stability and enabled spinning fibers with measurable mechanical properties. The further addition of PVA to the spinning dispersion provided additional stabilization as well as elongational viscosity. Comparison of fibers spun from concentrated supernatants and bulk mixtures showed that in spite of lower SWNT concentration, the more uniform microstructure of the concentrated supernatants resulted in better mechanical properties. The most remarkable fibers produced to date were from a concentrated LSZ–TTAB–SWNT supernatant combined with PVA. It retained 70% of lysozyme's native activity and demonstrated a remarkable toughness of 660.9 J g^{-1} which is four times greater than that of spider silk. It is expected that further refinements to the spinning and drying process will likely enable even better properties.

4. Experimental Section

Materials: The SWNT used in this research were UNIDYM (Sunnyvale, CA) batches 187.1 and 187.2 SWNT made via the high pressure carbon monoxide (HiPco) process. The SWNT had a purity of ≥99% as determined by thermogravimetric analysis. The average diameter was 1.24 nm and the average length was 1042 nm as determined by atomic force microscopy. Dialyzed, lyophilized LSZ from chicken egg white and TTAB were purchased from Sigma Aldrich (St. Louis, MO) and used as delivered. The LSZ was determined to be 90% pure via mass spectroscopy with the impurities being buffer salts of sodium acetate and sodium chloride. Polyvinyl alcohol (PVA), 99% hydrolyzed, with an average molecular weight of 195 000 g mol^{-1} and 99.3% purity was purchased from Sigma Aldrich and used as delivered. It should be noted that all solutions and dispersions were made using deionized (DI) water.

Sample Preparation: Dispersions of SWNT and LSZ were prepared using tip sonication of aqueous LSZ–SWNT dispersions. The sonication waves temporarily overcome the 0.5 eV nm^{-1} van der Waals force of attraction between SWNT allowing LSZ to intercalate and stabilize SWNT as individuals and small bundles. Since higher concentrations are desirable for processing into films and fibers, two sample preparation methods were investigated. First, the initial dispersions containing a mixture of individual SWNT and small aggregates were concentrated through evaporation on an orbital mixer in a small fume hood. Second, centrifugation of LSZ–SWNT dispersions at 17 000*g* for 3 h was used to remove excess SWNT and LSZ, leaving a supernatant of individual SWNT. The supernatants had much lower initial SWNT concentrations compared to the bulk dispersions, but were also concentrated by evaporation.

Dispersions of LSZ–SWNT stabilized with TTAB were prepared analogous to LSZ-SWNT. TTAB and LSZ were added to DI water and magnetically stirred for 10 min at which point SWNT was added and the dispersion was tip sonicated. Again, two sample preparation methods were used to create mixture and supernatant dispersions. After sonication, the mixture was processed by light centrifugation at 1000*g* for 30 min and discarding the bottom fraction prior to concentrating by evaporation. The supernatant was centrifuged for an additional 3 h at 17 000*g*. The mixture had a pH of 5.1 while the supernatant had a pH of 5.0. Evaporation of the LSZ–TTAB–SWNT dispersions was used to create concentrated samples for analysis and fiber spinning.

Dispersions of LSZ–SWNT or LSZ–TTAB–SWNT in PVA were created by combining dilute mixture or supernatant dispersions with solutions of PVA. The PVA solution was 5 wt% (4.10 vol%) in DI water mixed via magnetic stir bar at 50 °C for 3 days. After combination of the dispersions with the polymer solution, the resultant dispersions were mixed via magnetic stir bar for 20 minutes then concentrated via evaporation on an orbital mixer prior to fiber spinning. The following densities were used to calculate the volume fraction of individual constituents: SWNT–1.45 g cm^{-3}, LSZ–1.68 g cm^{-3}, and water –1.00 g cm^{-3}.

Atomic Force Microscopy (AFM): A Pacific Nanotechnology (Berkley, CA) Nano-R SPM was used for performing AFM to determine the average length and diameter of the pristine SWNT used during research. Approximately 5 µL of 0.25 wt% (0.15 vol%) DNA–0.01 wt% (0.007 vol%) SWNT supernatant was pipetted onto a cleaned, molecularly flat silicon stub and dried in a vacuum oven at 30 mmHg and 80 °C for 24 h. The AFM was operated in a static, non-contact mode. Each scan was of a 5 μm^2 area at a resolution of 256 and a scan speed of 0.5 Hz.

Scanning Electron Microscopy (SEM): A JEOL (Tokyo, Japan) 7000F FE-SEM with energy dispersive X-ray spectroscopy was used for performing SEM to qualitatively determine the presence of a molecular interaction between LSZ and SWNT. Dispersions of 0.5 wt% (0.3 vol%) LSZ–0.1 wt% (0.07 vol%) SWNT or 0.4 wt% (0.24 vol%) LSZ–0.4 wt% (0.28 vol%) SWNT–0.6 wt% (0.34 vol%) TTAB were mixed via vortex mixing and ≈10 µL were pipetted onto a clean, aluminum SEM sample stub. The sample was then vacuum dried at 30 mmHg and 80 °C for 24 h. After the sample was dried, it was gold-coated using a PELCO (Redding, CA) SC-6 Sputter Coater to increase the electrical conductance of the surface, which enhances the optical resolution.

Optical Microscopy: The optical microscope used in this research was a Nikon (Melville, NY) Eclipse 80i with transmitted light. Dispersion images were captured with LU Plan Fluor 20×/0.45 objective with 2.0× additional magnification in front of the camera for clarity. Optical microscopy was used to qualitatively determine the phase transition of LSZ–SWNT and LSZ–TTAB–SWNT dispersions and evaluate possible birefringence of the dispersion. Approximately 5 µL of 0.30 vol% LSZ–0.07 vol% SWNT or 0.24 vol% LSZ–0.28 vol% SWNT–0.34 vol% TTAB were pipetted onto a glass slide. To prevent evaporation, a glass cover slip was used, and the edges were sealed.

Absorption Spectroscopy: The absorption spectrometer used for this research was a Cary (Santa Clara, CA) 3E UV-vis Spectrophotometer. Scans were performed at room temperature at wavelengths from 200 nm to 800 nm at a scan rate of 600 nm s^{-1} and a resolution of 1 nm. Absorption spectroscopy was used to characterize the LSZ solutions and LSZ–SWNT dispersions, and quantitatively determine any shifts in absorption wavelength or intensity. Dispersions of 0.30 vol% LSZ–0.07 vol% SWNT or 0.24 vol% LSZ–0.28 vol% SWNT–0.34 vol%

TTAB were diluted at a ratio of 100 µL of dispersion to 5 mL of DI water and were then mixed via vortex mixing. Approximately 300 µL of LSZ solution or LSZ–SWNT dispersion were then pipetted into 1 mm pathlength quartz UV-vis cell for scanning. UV-vis was also used to determine antibacterial activity based on standard turbidimetric analysis. A 66 mM solution of potassium phosphate buffer was adjusted to a pH of 6.24 with potassium hydroxide at room temperature. Next, a bacterial cell suspension in the potassium phosphate buffer containing 0.015 wt% *Micrococcus lysodeikticus* was prepared. Then, 1 cm path length quartz cuvettes were filled with 2.5 mL of bacterial suspension, at which point 0.1 mL of buffer solution or dispersion was added. Finally, UV-vis spectroscopy was performed on the buffered bacterial suspension followed by UV-vis of a buffered bacterial suspension containing the dispersions where kinetic scans were run at 450 nm for 5 min.

Thermogravimetric Analysis (TGA): A TA Instruments (Waltham, MA) TGA Q50 was used to characterize nanotubes and dried dispersions. Mixture and supernatant dispersions were each prepared by removing water from the sample through non-heated, vacuum drying. After removal of the water, the remaining sample was placed in a sealed scintillation vial to prevent absorption of moisture. For testing, approximately 20 mg of sample was placed in a titanium sample pan to ensure adequate signal. Samples of each dispersion were run in air and in argon using the following test method: 1. Isothermal hold for 30 min, 2. Temperature ramp to 120 °C at 10 °C min^{-1}, 3. Isothermal hold at 120 °C for 30 min, 4. Temperature ramp to 800 °C at 10 °C min^{-1}, 5. Isothermal hold at 800 °C for 45 min.

Raman Spectroscopy: A Renishaw (Gloucesterchire, UK) inVia microRaman was used for Raman spectroscopy. Samples were prepared by drying in a vacuum oven for 24 h. The samples were then placed on double-sided tape attached to a glass slide. Prior to running test on all samples, each laser was calibrated using a silicon reference. Each sample was scanned by a 514 nm and 785 nm laser to probe both the semi-conducting and metallic CNT present. Each run by each laser consisted of 10 scans over a Raman shift from 100 cm^{-1} to 3200 cm^{-1}.

Mechanical Testing: An Instron (Norwood, MA) 5565 Calibration Lab was used to determine the mechanical properties of the fibers produced in this research. After the fibers were spun, samples were glued into a testing frame with a gauge length of 26 mm. The load cell used for this testing was 100 cN with a cross-head separation speed of 1.0 mm min^{-1}. The load and gauge length were balanced and zeroed before each run. Test data collected for each sample were load, extension, time, and strain. Analysis to determine specific mechanical properties was done using Excel.

Fiber Spinning: Wet and dry solution spinning were used to create fibers. The wet solution spinning involved the injection of LSZ–TTAB–SWNT dilute dispersions into a rotating coagulation bath of PVA followed by washing in DI water and air-drying. Before the coagulated fibers were completely dried, multiple individual fibers could be successively placed on top of one another causing the individual fibers to collapse into a single, larger fiber. The coagulation bath was rotated at 50 RPM and the 0.84 mm I.D. needle was injected 5 cm from the center with a tangential velocity of 26.6 cm s^{-1} and a volumetric rate of 0.34 mL min^{-1}. The dry solution spinning was carried out by injection of concentrated dispersions through 0.51 mm diameter needles into molds precut on a Teflon sheet at a volumetric rate of 0.5 mL min^{-1} (see the Supporting Information). Each fiber was allowed to air dry. Following drying, the fibers were removed from the molds for characterization. Post-process drawing of fibers was carried out through a manual pulley system. The draw ratio, final length over the initial length, for each fiber was six.

Supporting Information

Supporting Information is available from the Wiley Online Library or from the author.

Acknowledgements

We would like to acknowledge the National Science Foundation CAREER Award CMMI 0846629 for funding. We appreciate the assistance of Dr. Edward Davis with zeta potential measurements.

Received: January 19, 2013
Revised: May 1, 2013
Published online: July 9, 2013

[1] M. Dresselhaus, G. Dresselhaus, R. Saito, *Carbon* **1995**, *33*, 883.
[2] Research America, Infectious Disease, *Mary Woodard Lasker Charitable Trust* Alexandria, VA **2004**, p. 1.
[3] A. Caro, V. Humblot, C. Methivier, M. Minier, M. l. Salmain, C.-M. Pradier, *J. Phys. Chem. B* **2009**, *113*, 2101.
[4] D. W. Horn, K. Tracy, C. J. Easley, V. A. Davis, *J. Phys. Chem. C* **2012**, *116*, 10341.
[5] D. Nepal, K. E. Geckeler, *Small* **2007**, *3*, 1259; D. Nepal, K. E. Geckeler, *Small* **2006**, *2*, 406.
[6] D. Nepal, S. Balasubramanian, A. L. Simonian, V. A. Davis, *Nano Lett.* **2008**, *8*, 1896.
[7] D. Nepal, M. L. Minus, S. Kumar, *Macromol. Biosci.* **2011**, *11*, 875.
[8] S. Dölle, B.-D. Lechner, J. H. Park, S. Schymura, J. P. F. Lagerwall, G. Scalia, *Angew. Chem. Int. Ed.* **2012**, *51*, 3254.
[9] a) M. J. O'Connell, P. Boul, L. M. Ericson, C. Huffman, Y. Wang, E. Haroz, C. Kuper, J. Tour, K. D. Ausman, R. E. Smalley, *Chem. Phys. Lett.* **2001**, *342*, 265; b) A. Hartschuh, H. N. Pedrosa, L. Novotny, T. D. Krauss, *Science* **2003**, *301*, 1354.
[10] B. Vigolo, A. Penicaud, C. Coulon, C. Sauder, R. Pailler, C. Journet, P. Bernier, P. Poulin, *Science* **2000**, *290*, 1331.
[11] P. Poulin, B. Vigolo, P. Launois, *Carbon* **2002**, *40*, 1741.
[12] a) Z. Sun, V. Nicolosi, D. Rickard, S. D. Bergin, D. Aherne, J. N. Coleman, *J. Phys. Chem. C* **2008**, *112*, 10692; b) B. White, S. Banerjee, S. O'Brien, N. J. Turro, I. P. Herman, *J. Phys. Chem. C* **2007**, *111*, 13684.
[13] J. N. Coleman, *Adv. Funct. Mater.* **2009**, *19*, 3680.
[14] J. N. Israelachvili, *Intermolecular and surface forces*, Academic Press, London **1992**.
[15] A. Bordbar, R. Hosseinzadeh, M. Norozi, *J. Therm. Anal. Calorim.* **2007**, *87*, 453.
[16] a) K. Hayashi, M. Kugimiya, T. Imoto, M. Funatsu, C. C. Bigelow, *Biochemistry* **1968**, *7*, 1467; b) K. Hayashi, M. Kugimiya, T. Imoto, M. Funatsu, C. C. Bigelow, *Biochemistry* **1968**, *7*, 1461.
[17] M. Subramanian, B. Sheshadri, M. Venkatappa, *J. Biosci.* **1986**, *10*, 359.
[18] a) V. Karachevtsev, A. Plokhotnichenko, M. Karachevtsev, V. Leontiev, *Carbon* **2010**, *48*, 3682; b) H. Edelhoch, *Biochemistry* **1967**, *6*, 1948.
[19] B. S. Shim, J. Zhu, E. Jan, K. Critchley, S. Ho, P. Podsiadlo, K. Sun, N. A. Kotov, *ACS Nano* **2009**, *3*, 1711.
[20] A. B. Dalton, S. Collins, E. Munoz, J. M. Razal, V. H. Ebron, J. P. Ferraris, J. N. Coleman, B. G. Kim, R. H. Baughman, *Nature* **2003**, *423*, 703.
[21] a) A. B. Dalton, S. Collins, J. Razal, E. Munoz, V. H. Ebron, B. G. Kim, J. N. Coleman, J. P. Ferraris, R. H. Baughman, *J. Mater. Chem.* **2004**, *14*, 1; b) J. N. Barisci, M. Tahhan, G. G. Wallace, S. Badaire, T. Vaugien, M. Maugey, P. Poulin, *Adv. Funct. Mater.* **2004**, *14*, 133; c) B. Vigolo, P. Poulin, M. Lucas, P. Launois, P. Bernier, *Appl. Phys. Lett.* **2002**, *81*, 1210.
[22] a) F. Duboeuf, H. Liebgott, A. Basarab, E. Brusseau, P. Delachartre, D. Vray, Static mechanical assessment of elastic Young's modulus of tissue mimicking materials used for medical imaging, 29th Annual International Conference of the IEEE **2007**, DOI: 10.1109/IEMBS.2007.4353073; b) H. Möller, S. Grelier, P. Pardon, V. Coma, *J. Agric. Food Chem.* **2004**, *52*, 6585.

[23] T. Liu, S. Kumar, *Nano Lett.* **2003**, *3*, 647.
[24] L. A. Pottick, **1986**.
[25] a) T. Cooney, L. Wang, S. Sharma, R. Gauldie, A. Montana, *J. Polym. Sci., Part B: Polym. Phys.* **1994**, *32*, 1163; b) M. T. Islam, N. Rodríguez-Hornedo, S. Ciotti, C. Ackermann, *Pharm. Res.* **2004**, *21*, 1844.
[26] a) V. Z. Poenitzsch, D. C. Winters, H. Xie, G. R. Dieckmann, A. B. Dalton, I. H. Musselman, *J. Am. Chem. Soc.* **2007**, *129*, 14724; b) A. Rao, P. Eklund, S. Bandow, A. Thess, R. E. Smalley, *Nature* **1997**, *388*, 257.
[27] M. S. Dresselhaus, G. Dresselhaus, P. Eklund, D. E. H. Jones, *Science of fullerenes and carbon nanotubes*, Vol. *965*, Academic Press, New York **1996**.
[28] K. R. Moonoosawmy, P. Kruse, *J. Am. Chem. Soc.* **2008**, *130*, 13417.
[29] P. M. Ajayan, L. S. Schadler, C. Giannaris, A. Rubio, *Adv. Mater.* **2000**, *12*, 750.
[30] T. Chatterjee, K. Yurekli, V. G. Hadjiev, R. Krishnamoorti, *Adv. Funct. Mater.* **2005**, *15*, 1832.
[31] S. M. Bachilo, M. S. Strano, C. Kittrell, R. H. Hauge, R. E. Smalley, R. B. Weisman, *Science* **2002**, *298*, 2361.
[32] M. J. O'Connell, S. Sivaram, S. K. Doorn, *Phys. Rev. B* **2004**, *69*, 235415.
[33] P. Corio, A. Jorio, N. Demir, M. Dresselhaus, *Chem. Phys. Lett.* **2004**, *392*, 396.
[34] H. M. Ding, L. Shao, R. J. Liu, Q. G. Xiao, J. F. Chen, *J. Colloid Interface Sci.* **2005**, *290*, 102.
[35] D. Merli, M. Ugonino, A. Profumo, M. Fagnoni, E. Quartarone, P. Mustarelli, L. Visai, M. S. Grandi, P. Galinetto, P. Canton, *J. Nanosci. Nanotechnol.* **2011**, *11*, 3100.
[36] C. A. Dyke, J. M. Tour, *J. Phys. Chem. A* **2004**, *108*, 11151.
[37] a) L. Collins, C. Dawes, *J. Dental Res.* **1987**, *66*, 1300; b) C. Hannig, J. Hoch, K. Becker, M. Hannig, T. Attin, *Arch. Oral Biol.* **2005**, *50*, 821.